

## Application of computational fluid dynamics analysis for improving performance of commercial scale selective catalytic reduction

Jin Man Cho<sup>†</sup>, Jeong-Woo Choi\*, Sung Ho Hong\*\*, Kwang Chu Kim\*\*, Jung Hee Na\*\* and Jun Yub Lee\*\*

Department of Chemical & Biomolecular Engineering,

\*Department of Chemical & Biomolecular Engineering and Interdisciplinary Program of Integrated Biotechnology, Sogang University, #1 Sinsu-dong, Mapo-gu, Seoul 121-742, Korea

\*\*Korea Power Engineering Company, INC. 360-9 Mabuk-ri, Guseong-eup, Yongin-si, Gyeonggi-do 449-713, Korea  
(Received 28 February 2005 • accepted 8 August 2005)

**Abstract**—The performance of commercial scale selective catalytic reduction (SCR) system is strongly dependant upon the degree of mixing between  $\text{NH}_3$  and  $\text{NO}_x$  or  $\text{NH}_3$  concentration distribution at the catalyst layer according to the reaction kinetics of SCR catalysts. Insufficient mixing of the reduction agent and  $\text{NO}_x$  mass flow necessitates an uneconomically large catalyst volume and high  $\text{NH}_3$  slip to meet the required  $\text{NO}_x$  emission values. The effective methodology which can increase the performance of commercial scale SCR through improving  $\text{NH}_3$  concentration distribution at the catalyst layer using computational fluid dynamics (CFD) analysis was suggested and applied to the real operations. The operation results have shown that the performance of commercial SCR was improved from 54.4% to 74.8% as  $\text{NH}_3$  concentration deviation at the catalyst layer was reduced from 23.6% to 8.6%. It is established that the increase of  $\text{NH}_3$  concentration uniformity at the catalyst layer contributes to improvement of performance of commercial scale SCR.

Key words: Commercial Scale Selective Catalytic Reduction, Computational Fluid Dynamics,  $\text{NO}_x$ ,  $\text{NH}_3$  Concentration Distribution

### INTRODUCTION

Various  $\text{NO}_x$  treatment systems for pollution sources such as industrial plants and power plants have been installed to meet the reinforced restriction and limitation for atmospheric pollutants. Selective catalyst reduction (SCR) is an effective treatment system used worldwide for large-scale plants [Arbind, 1995; Bruce, 1995; Jaime, 1993; Kotter and Lintz, 1991]. The performance of an SCR system depends on the catalysts and the operation parameters. SCR operating parameters are reaction temperature, space velocity (SV), flue gas components,  $\text{NH}_3/\text{NO}_x$  molar ratio, the limitation of  $\text{NH}_3$  slip, SCR operation time and the degree of mixing between  $\text{NH}_3$  and  $\text{NO}_x$  or  $\text{NH}_3$  distribution at the catalyst layer [Ralf et al., 2003]. Except for the degree of mixing between  $\text{NH}_3$  and  $\text{NO}_x$  or  $\text{NH}_3$  distribution, other operation parameters of existing SCR systems are restricted in improving or modifying because those need additional costs and bring about a drop in efficiency of existing main plants and there are many limitations in retrofitting. The degree of mixing between  $\text{NH}_3$  and  $\text{NO}_x$  or  $\text{NH}_3$  concentration distribution has a margin for improvement in a large-scale SCR system. According to the reaction kinetics of SCR catalysts, the effectiveness of the SCR process is strongly dependent upon the degree of mixing between  $\text{NH}_3$  and  $\text{NO}_x$  or  $\text{NH}_3$  concentration distribution at the catalyst layer [Freek et al., 1993; Jiri et al., 1993]. Insufficient mixing of the reducing agent and  $\text{NO}_x$  mass flow necessitates an uneconomically large catalyst volume and high  $\text{NH}_3$  slip to meet the required  $\text{NO}_x$  emission values. The static mixer at downstream of ammonia injection grid (AIG) and guide vanes at upstream of catalyst layer as a flow

correction device are installed in the coal fired power plant in order to obtain the uniform  $\text{NH}_3$  concentration distribution at the catalyst layer [Heck et al., 1994; Kenneth and John, 1993; Kevin et al., 1999]. The combined cycle power plant does not need additional SCR reactor because catalyst layer and AIG should be installed inside heat recovery steam generators (HRSG). In addition, it is difficult to install flow correction devices because those cause additional pressure drop to reduce the efficiency of power generation [Kokkinos et al., 1999]. In general, an SCR system in combined cycle power plant should obtain uniform  $\text{NH}_3$  concentration distribution at the catalyst layer without additional flow correction devices. Therefore, it is important to find the optimal AIG location, where flue gas behavior is uniform, in order to obtain a uniform  $\text{NH}_3$  concentration distribution at the catalyst layer. The flue gas behavior in HRSG becomes uniform during passing through heat pipe bundles. The catalyst layer should be installed in the region in the middle region of heat pipe bundles. In many cases, the AIG is installed in HRSG inlet expansion duct region, which has non-uniform flue gas behavior. In these cases, it is difficult to get the uniform  $\text{NH}_3$  concentration distribution at the catalyst layer.

In this study, an effective methodology which can increase the performance of commercial scale SCR in combined cycle power plant was suggested and applied to real operations. An analytic method using computational fluid dynamics (CFD) was introduced. Flue gas mass fluxes passing through individual AIG groups were calculated by CFD analysis. And the optimal  $\text{NH}_3$  feed rates for individual AIG groups to form the uniform  $\text{NH}_3$  concentration distribution at the catalyst layer were determined according to the flue gas mass fluxes. In the course of CFD analysis,  $\text{NH}_3$  concentration deviation,  $D_c$  at the catalyst layer was defined and calculated for all cases of experiments in order to analyze the relationship with  $\text{NO}_x$

<sup>†</sup>To whom correspondence should be addressed.  
E-mail: zozinman@mobilis.co.kr

**Table 1. Catalyst specifications**

Type	Honeycomb	Production method	Extrusion
Number of cells (CPSI)	35	Perforation ratio (%)	$\geq 72$
Length (mm)	$140 \pm 2 / 550 \pm 2$	Torsion (mm)	$\leq 1.3$
Outer length (mm)	$150 \pm 2$		$\leq 1.5$
Thickness of outer wall (mm)	$\leq 1.3$	Contact area ( $\text{m}^2/\text{m}^3$ )	$\geq 792$
Thickness of inner wall (mm)	$0.65 \pm 0.05$	Bulk density ( $\text{kg}/\text{m}^3$ )	$550 \pm 2$

removal efficiency.

## EXPERIMENTAL APPARATUS AND PROCEDURE

### 1. SCR Catalyst

The specifications of the extruded honeycomb catalyst used in this study are described in Table 1. It consists of  $\text{TiO}_2/\text{Mn}$  oxides. The catalyst elements are combined into carbon steel boxes called modules, which are designed primarily with a view to permanently ensuring an operationally suitable arrangement of the catalysts in the reactor.

### 2. Commercial Scale SCR

The commercial scale SCR system is installed in horizontal type heat recovery steam generator (HRSG) of a combined cycle power plant. It consists of  $\text{NH}_3$  unloading and storage part,  $\text{NH}_3$  injection part and SCR catalyst layer and accessories part. The system configuration is shown in Fig. 1. The flue gas flow rate is  $800,000 \text{ Nm}^3/\text{hr}$  (based on standard of design). The catalyst layers consist of two layers, 1<sup>st</sup> catalyst layer ( $22 \text{ m}^3$ ) and 2<sup>nd</sup> catalyst layer ( $44 \text{ m}^3$ ). And 1<sup>st</sup> catalyst layer has two sub-layers, which have  $11 \text{ m}^3$  of catalyst, respectively. The total volume of catalyst is  $66 \text{ m}^3$ . Therefore, SV of commercial scale SCR is  $12,121 \text{ hr}^{-1}$ . Fig. 2 shows the location of catalyst layers and their specification. Fig. 3 shows AIG in commercial scale SCR.

### 3. Procedure

#### 3-1. Performance Tests Using Individual AIG Group

The objective of this test is to investigate the flue gas mass flux behavior in HRSG and the relationship between performance and  $\text{NH}_3$  concentration deviation experimentally.  $\text{NH}_3$  gas was allowed to feed from only one AIG group for each test. Duration for each test was 30 minutes after previous operation for 30 minutes to stabilize the SCR system, and inlet  $\text{NO}_x$ , outlet  $\text{NO}_x$  concentration and  $\text{NH}_3$  slip were monitored at one minute intervals. Total  $\text{NH}_3$  feed rate was maintained constantly by setting  $\text{NH}_3$  gas flow control valve during the period of whole tests.

#### 3-2. Performance Tests Using All AIG Groups

The performance test operations using all AIG groups were implemented in order to evaluate effectiveness of the proposed method which can form the uniform  $\text{NH}_3$  concentration distribution at the catalyst layer using CFD analysis. The number of operation cases is four. The first case experiment is to apply the same  $\text{NH}_3$  feed rate for all AIG's groups. And the other experiments are to apply different  $\text{NH}_3$  feed rates for individual AIG's groups, which were determined based on flue gas mass flux passing through individual AIG groups obtained from CFD analysis result. In these tests, SCR control system logic was set up to let  $\text{NH}_3$  slip to be maintained at 10 ppm and the total  $\text{NH}_3$  feed rate was controlled automatically according to inlet  $\text{NO}_x$  concentration. For each case, twice opera-

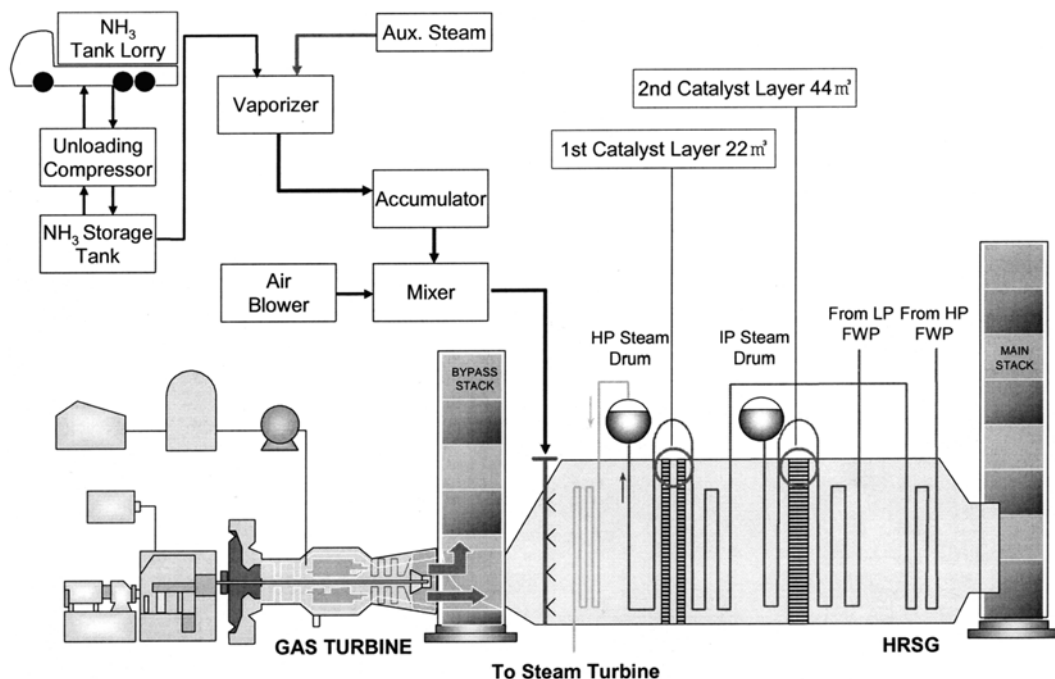


**Fig. 1. Commercial scale SCR system configuration.**

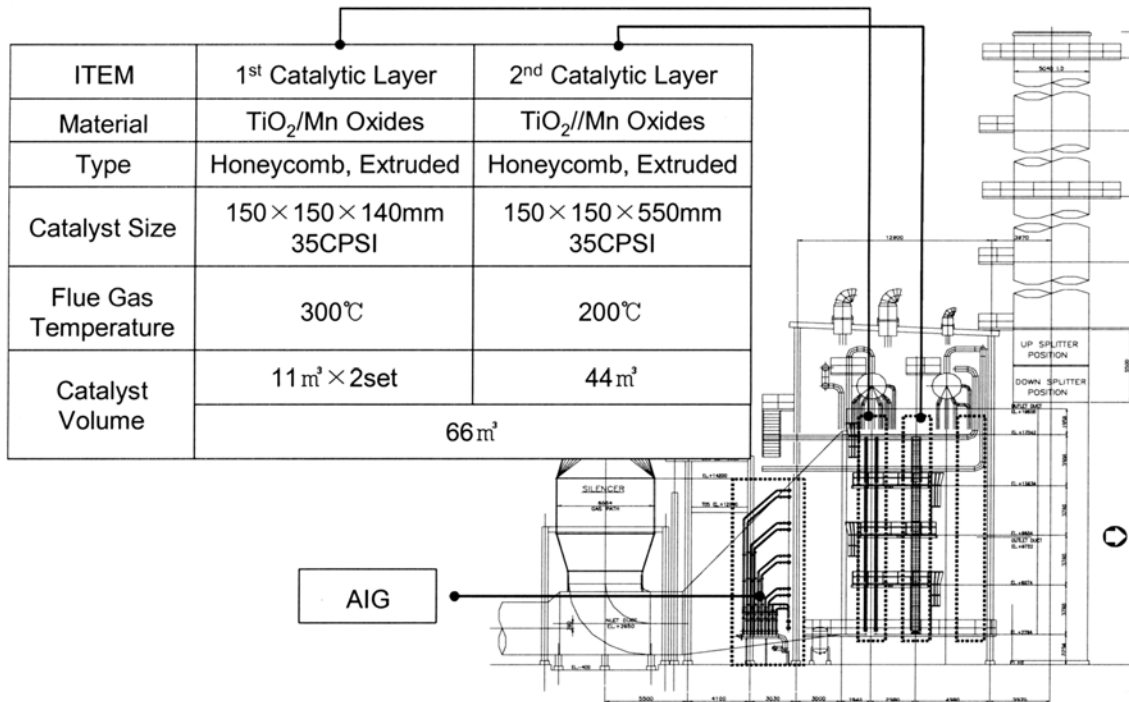


Fig. 2. The catalyst layers in commercial scale SCR system.

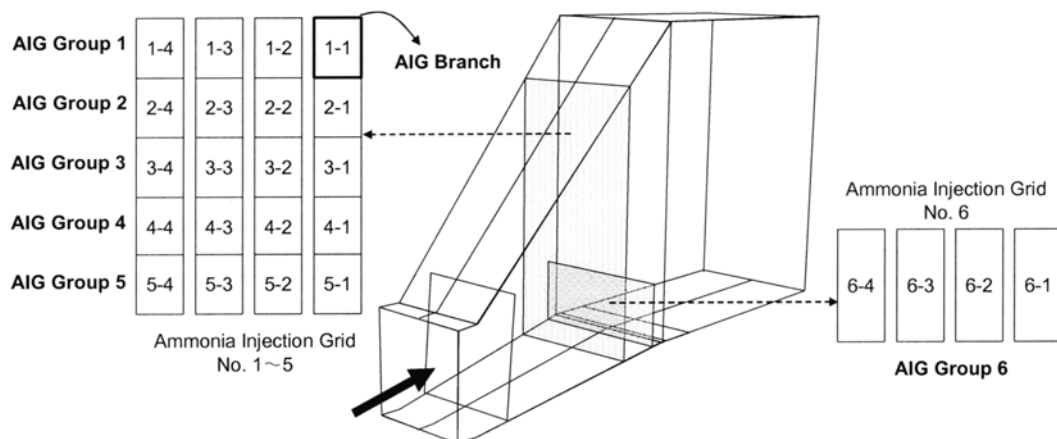


Fig. 3. Ammonia injection grid groups and branches of commercial scale SCR.

tions were implemented and each operation was maintained for 2 hours. Inlet NO<sub>x</sub>, outlet NO<sub>x</sub> concentration and NH<sub>3</sub> slip were also measured at one minute intervals.

## COMPUTATIONAL FLUID DYNAMICS ANALYSIS

### 1. CFD Analysis for Commercial Scale SCR in HRSG

Computational domain for fluid dynamics calculation is defined. The governing equations for physical properties such as velocity, pressure and temperature are derived by means of applying mass, momentum and energy conservation theory. However, it is impossible to obtain an analytic solution by manual calculation method no matter how simple the case is because these are non-linear partial derivative equations. Therefore, computational fluid dynamics analysis method has been introduced as an alternative [Adams et al.,

2002; Kevin et al., 2000; Sayre and Milobowski, 1999].

The existing plants such as thermal power plants and incinerators which need SCR system have expansion or reduction section due to catalyst layer, AIG bypass duct installation in course of retrofitting. Especially, it is necessary to equip with catalyst layers and AIG into HRSG in case of a combined cycle power plant; thus, flue gas behavior passing through the catalyst layer must be changed by inlet expansion duct, flow correction devices and heat pipe bundles. It is necessary to determine the optimal location of AIG to equip with additional guide vanes or to regulate NH<sub>3</sub> feed rates of individual AIG branches for a uniform NH<sub>3</sub> concentration distribution at the catalyst layer. A physical model test or numerical analysis can be used to predict the result of these modification.

### 2. Governing Equations

The following are mass, momentum and scalar conservation equa-

tions.

*Mass Conservation*

$$\frac{\partial \rho}{\partial t} + \frac{\partial(\rho u_i)}{\partial x_i} = S_m \quad (1)$$

*Momentum Conservation*

$$\frac{\partial(\rho u_i)}{\partial t} + \frac{\partial(\rho u_i u_j)}{\partial x_j} = -\frac{\partial p}{\partial x_i} + \frac{\partial}{\partial x_j} \left[ \mu \left( \frac{\partial u_i}{\partial x_j} + \frac{\partial u_j}{\partial x_i} \right) \right] + \rho g_i + F_i \quad (2)$$

*Scalar Conservation*

$$\frac{\partial(\rho \phi)}{\partial t} + \frac{\partial(\rho u_i \phi)}{\partial x_i} = \frac{\partial}{\partial x_j} \left( \Gamma \frac{\partial \phi}{\partial x_j} \right) + S_\phi \quad (3)$$

### 3. Finite Volume Element Method [Pantankar, 1980]

Discretization of governing equations is as follows. For one dimensional system and steady state, scalar  $\phi$  conservation equation is given as Eq. (4).

$$\frac{\partial(\rho u \phi)}{\partial x} = \frac{\partial}{\partial x} \left( \Gamma \frac{\partial \phi}{\partial x} \right) + S_\phi \quad (4)$$

For one cell, by integrating Eq. (4) and applying divergence theorem, convection term of the left side is changed into Eq. (5).

$$\int_{\text{Volume } V} \frac{\partial(\rho u \phi)}{\partial x} dV = \int_{\text{surface } A} \rho u \phi dA = (\rho u \phi)_e - (\rho u \phi)_w \quad (5)$$

Diffusion term and source term of the right side are changed into Eq. (6).

$$\int_{\text{volume } V} \left[ \frac{\partial}{\partial x} \left( \Gamma \frac{\partial \phi}{\partial x} \right) + S_\phi \right] dV = \left( \Gamma \frac{\partial \phi}{\partial x} \right)_e - \left( \Gamma \frac{\partial \phi}{\partial x} \right)_w + S_\phi \Delta V \quad (6)$$

The value of  $\phi$  and  $\partial\phi/\partial x$  at locations between one cell and neighbor cell should be calculated in the center because all variables are stored in the center of cell. First order upwind scheme, power-law scheme and second order upwind scheme are used in calculating these values [Fluent User's Guide, 1996]. By means of calculating Eq. (6) for each cells and combining, Eq. (7) as a matrix equation can be obtained.

$$a_p \phi_p = \sum_{nb} a_{nb} \phi_{nb} + b \quad (7)$$

where, nb is neighbor cells of one cell. In case of two dimensional rectangular mesh the number of neighbor cells is four and in case of three dimensional system it is six. As  $a_p$  and  $a_{nb}$  are the function of  $\phi$ , the solution for non-linear equation can be obtained by iteration method.

### 4. SIMPLE Algorithm and Numerical Schemes

The pressure correction equation of simple-implicit method for pressure-linked equation (SIMPLE) algorithm used in FLUENT™ is obtained from modifying mass and momentum conservation equations. The mass and momentum equations should be calculated in order to analyze flue gas behavior and the transfer equation for 1 chemical species should be calculated in order to analyze the injected air and the NH<sub>3</sub> concentration distribution. Standard  $k-\epsilon$  model [Lauder and Spalding, 1972] is used as a turbulence model. The density is obtained from volume ratio of each chemical species and temperature. The values for average temperature at the region of calculation are adopted as other physical properties.

### 5. Meshes

January, 2006

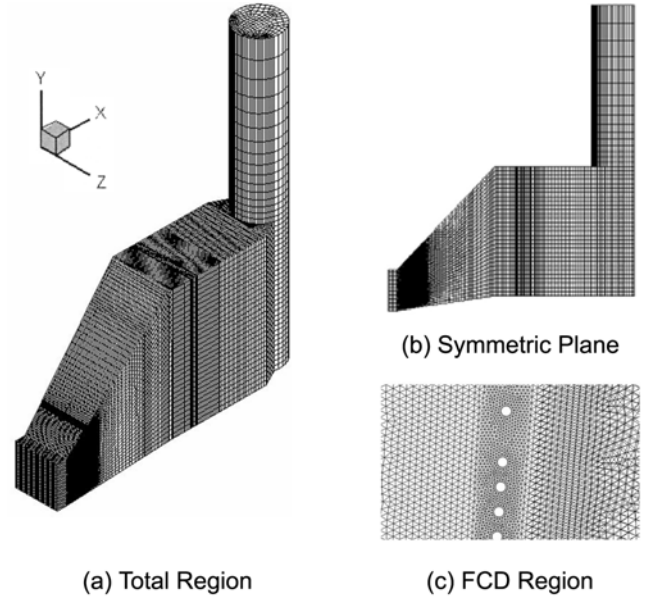


Fig. 4. Meshes for CFD analysis.

Fig. 4 shows meshes for analyzing flue gas behavior and NH<sub>3</sub> concentration distribution in commercial scale SCR. CFD analysis was done for half of the total region because horizontal HRSG is a symmetric structure. The meshes consist of about 200,000 hexahedral and pentahedral cells and are clustered near wall, porous media and FCD region to increase accuracy.

### 6. Porous Media

HRSG consists of several heat exchangers which have numerous heat pipe bundles. The meshes should be prepared according to the real shapes of pipe bundles and they should be included in calculation for complete analysis. However, it is impossible to calculate in considering present computer ability. Therefore, the regions of heat pipe bundles and catalyst layer are considered as porous media in this study. To verify the feasibility for porous media assumption CFD analysis was implemented for three cases which have different resistance coefficients in heat pipe bundles such as  $C_v = C_h$ ,  $C_v = 0.5C_h$  and  $C_v = 0.1C_h$ .  $C_v$  is vertical direction (Y-axis) resistance coefficient and  $C_h$  is horizontal direction (X-axis) resistance coefficient. However, flue gas cannot flow toward vertical direction in the catalyst layer because the catalyst is honeycomb type.

In CFD analysis, numerical approach for porous media is treated as momentum source term of general fluid flow equation and this source term consists of viscous loss term and inertial loss term based on Darcy's law.

$$S_i = \nabla p = \sum_{j=1}^3 D_{ij} \mu V_j + \sum_{j=1}^3 C_{ij} \frac{1}{2} \rho V_j |V_j| \quad (8)$$

Calculating the source term determines the pressure drop in the porous region and the pressure drop is proportional to fluid velocity in cells.

In case of simple porous media which has the same value for X, Y and Z direction, Eq. (8) can be simplified like Eq. (9).

$$\nabla p = \frac{\mu}{\alpha} V_i + C_2 \left( \frac{1}{2} \rho V_i |V_i| \right) \quad (9)$$

In general, it is not necessary to consider permeability in case of pipe bundles and porous plate; thus, only  $C_2$  should be calculated and it can be obtained from Eq. (10).

$$C_2 = \frac{K'_L}{T} \tag{10}$$

The relationship between  $K'_L$  and  $K_L$  can be given such as Eq. (11) in case of full opening.

$$K'_L = K_L \left( \frac{V^2_{actual\ open}}{V^2_{100\% open}} \right) = K_L \left( \frac{A_{actual\ open}}{A_{100\% open}} \right) \tag{11}$$

In case of 100% opening,  $K_L$  can be obtained from Eq. (12)

$$K_L = \frac{\Delta p}{\frac{1}{2} \rho V^2} \tag{12}$$

### 7. CFD Analysis for Flue Gas Behavior

Average flue gas mass flux,  $\rho V_x$  passing through the AIG is calculated from the result of CFD analysis. It can be considered as NOx amount which should react with  $NH_3$  because NOx concentration is a constant value in flue gas. Therefore,  $NH_3$  feed rates for individual AIG groups can be determined based on average flue gas mass flux passing through the AIG. And also  $D_m$  as a flue gas distribu-

tion deviation parameter in Eq. (13) is introduced to evaluate the uniformity of flue gas behavior.  $D_m$  is calculated at AIG and catalyst layers.

$$D_m = \sqrt{\left( \frac{\int (\rho_w - \bar{\rho}_w)^2 dA}{A} \right)} / \sqrt{\bar{\rho}_w} \times 100\% \tag{13}$$

### 8. CFD Analysis for $NH_3$ Concentration Distribution

CFD analysis for  $NH_3$  concentration distribution was implemented for all operation cases assuming the ratio of resistance coefficients is  $C_v=0.5C_h$ .  $NH_3$  concentration distribution deviation parameters ( $D_c$ ) for total region including catalyst layer are calculated. The homogeneity of  $NH_3$  concentration at the catalyst layer can be evaluated from  $D_c$ .  $D_c$  is defined as Eq. (14) and the relationship between  $D_c$  and the performance of commercial scale SCR was analyzed.

$$D_c = \sqrt{\left( \frac{\int (c - \bar{c})^2 dA}{A} \right)} / \sqrt{\bar{c}} \times 100\% \tag{14}$$

## RESULTS AND DISCUSSION

### 1. CFD Analysis

#### 1-1. Temperature and Pressure Distribution inside HRSG

Fig. 5 shows the flue gas temperature distribution of HRSG equip-

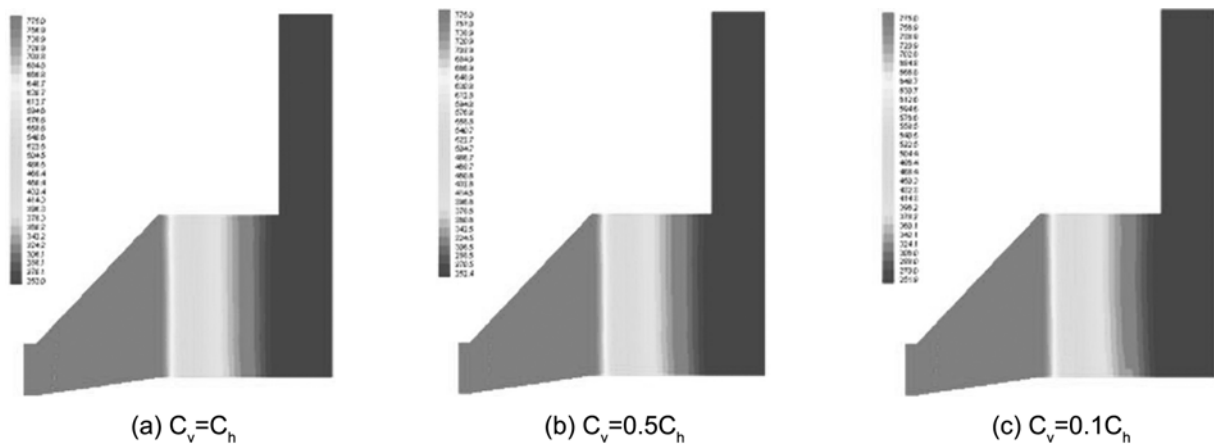


Fig. 5. CFD analysis result for flue gas temperature distribution (°K) at the HRSG symmetric plane.

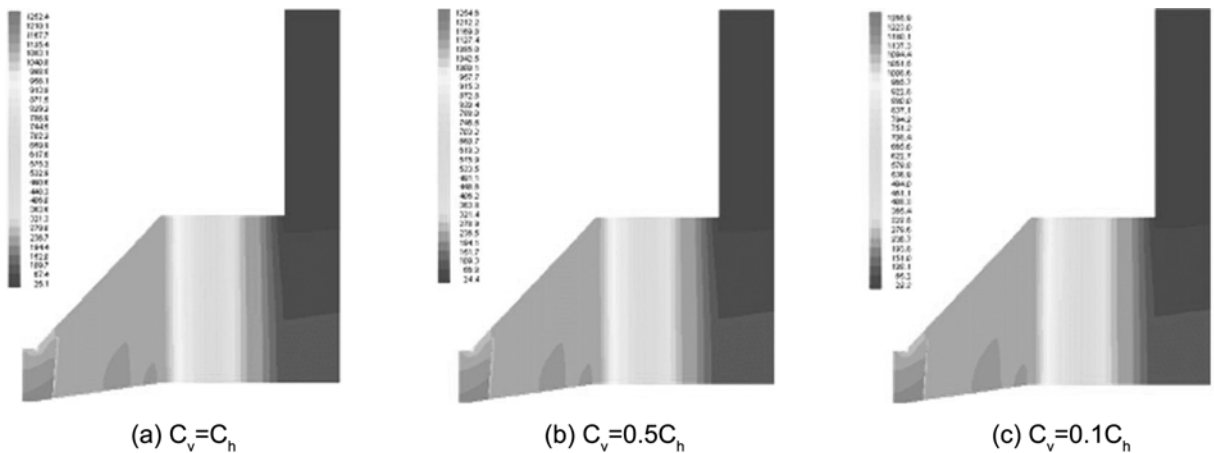


Fig. 6. CFD analysis result for flue gas pressure distribution (mmH<sub>2</sub>O) at the HRSG symmetric plane.

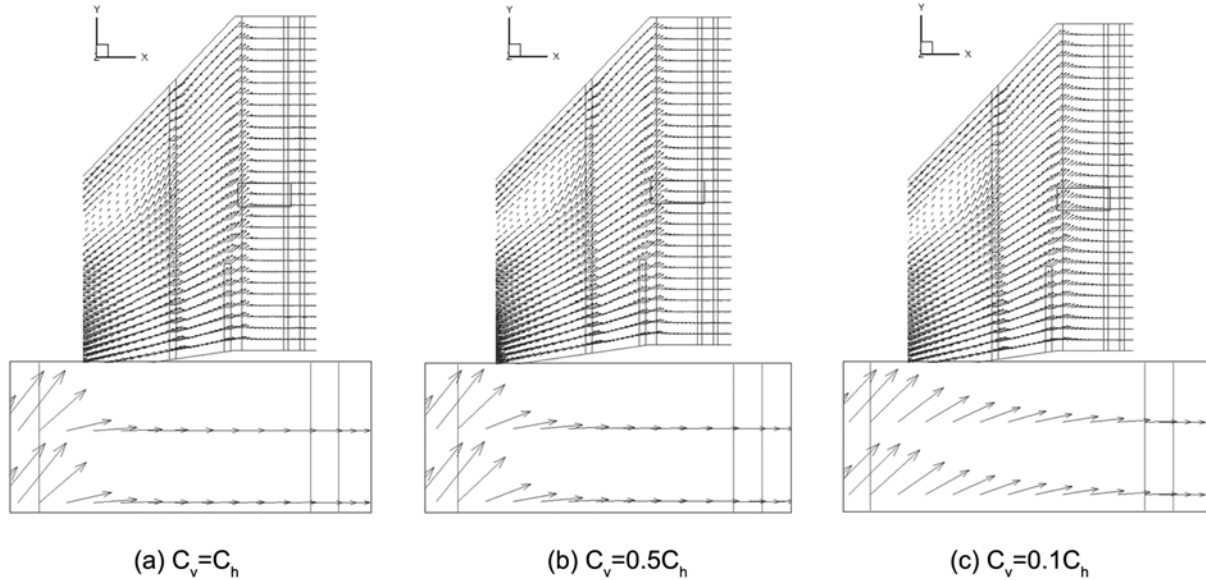


Fig. 7. Velocity vector in AIG and catalyst layer region.

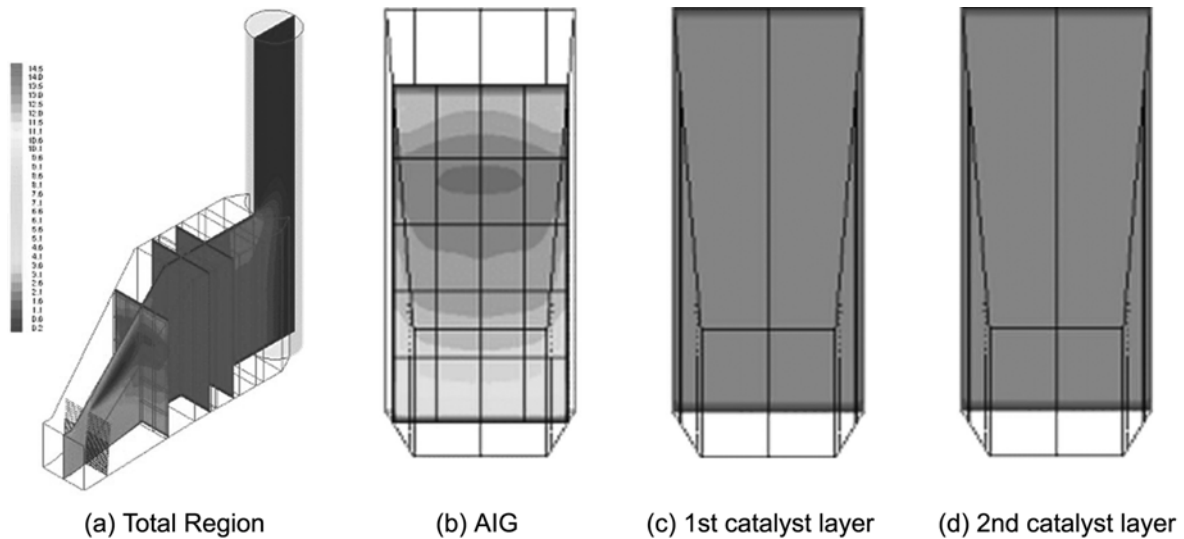


Fig. 8. Flue gas mass flux,  $\rho V_x$  ( $\text{kg}/\text{m}^2 \cdot \text{sec}$ ) distribution for  $C_v = C_h$ .

ped with commercial scale SCR for  $C_v = C_h$ ,  $C_v = 0.5C_h$  and  $C_v = 0.1C_h$ . Temperature is decreased by heat exchange between flue gas and heat pipe bundles as flue gas flows toward the stack. Fig. 6 shows the flue gas pressure distribution of HRSG for  $C_v = C_h$ ,  $C_v = 0.5C_h$  and  $C_v = 0.1C_h$ . And also pressure is decreased by pressure drop due to heat pipe bundles and catalyst layers.

#### 1-2. Flue Gas Behavior

Fig. 7(a), (b) and (c) show flue gas velocity vector plots at the symmetric plane for  $C_v = C_h$ ,  $C_v = 0.5C_h$  and  $C_v = 0.1C_h$ , respectively. It can be seen that there is rapid upward flow ( $V_y$ ) around the first heat exchanger, high pressure superheater (HPSH) and this leads to uniform flue gas flowing in the downstream region. It can be observed that as the vertical resistance coefficient becomes smaller, the upward flow of flue gas is stronger in the HPSH region. The upward flow of flue gas of the low part of HRSG is stronger than that of the upper part of HRSG. After passing through HPSH, the

main flowing direction velocity ( $V_x$ ) becomes dominant and the other direction velocities ( $V_y$ ,  $V_z$ ) become tiny. Figs. 8, 9 and 10 show flue gas mass flux,  $\rho V_x$  distribution for  $C_v = C_h$ ,  $C_v = 0.5C_h$  and  $C_v = 0.1C_h$ , respectively. It shows that as flue gas flows toward stack its distribution becomes uniform. Table 2 shows  $V_x$ ,  $\rho V_x$  and  $\rho V_x$  deviation  $D_m$  for  $C_v = C_h$ ,  $C_v = 0.5C_h$  and  $C_v = 0.1C_h$ . Fig. 11 shows variation of  $D_m$  values at AIG 1<sup>st</sup> catalyst layer and 2<sup>nd</sup> catalyst layer for  $C_v = C_h$ ,  $C_v = 0.5C_h$  and  $C_v = 0.1C_h$ .  $D_m$  values are decreased as flue gas flows toward stack. As  $C_v$  becomes smaller, the upward flow of flue gas has a tendency to be stronger and  $D_m$  at the same location is increased. The range of  $D_m$  at the AIG for  $C_v = C_h$ ,  $C_v = 0.5C_h$  and  $C_v = 0.1C_h$  is 24.3-25.8% and it is much greater than that of  $D_m$  at the catalyst layers. It means that flue gas behavior at catalyst layer is more uniform than that at the AIG.

Compared with the amount of flue gas, the amount of  $\text{NH}_3$  gas with air injected into HRSG through the AIG is very small. There-

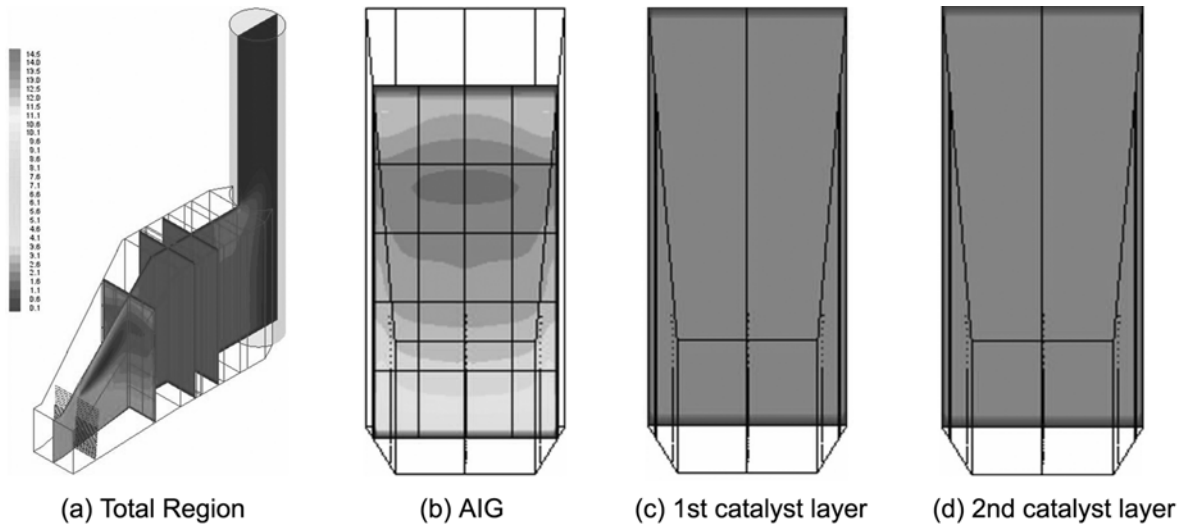


Fig. 9. Flue gas mass flux,  $\rho V_x$  ( $\text{kg}/\text{m}^2 \cdot \text{sec}$ ) distribution for  $C_v=0.5C_h$ .

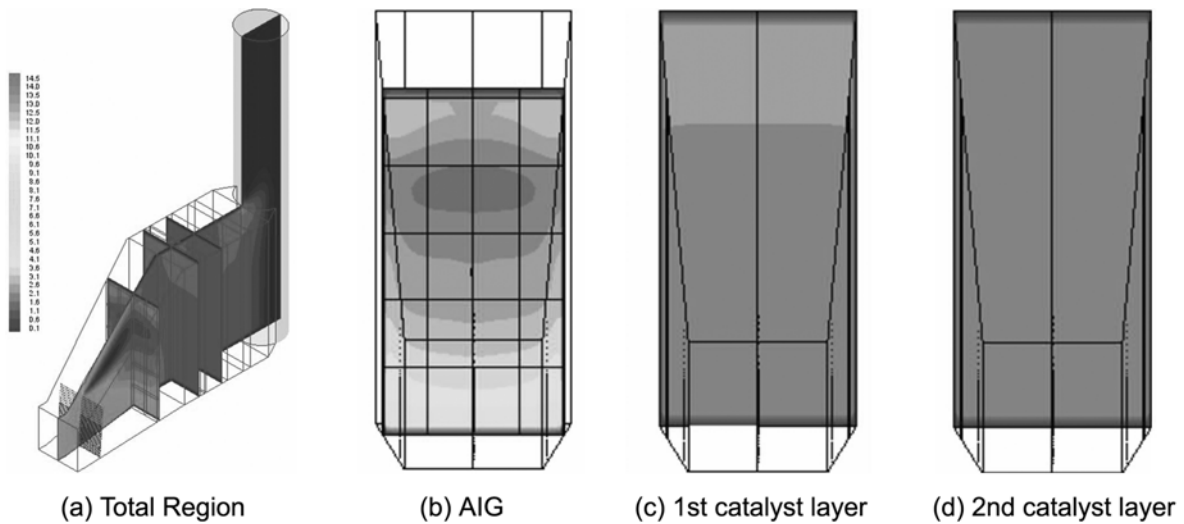


Fig. 10. Flue gas mass flux,  $\rho V_x$  ( $\text{kg}/\text{m}^2 \cdot \text{sec}$ ) distribution for  $C_v=0.1C_h$ .

**Table 2. CFD result for flue gas velocity ( $V_x$ ), mass flux ( $\rho V_x$ ) and mass flux deviation ( $D_m$ ) in horizontal type HRSG**

Location	Item	$C_v=C_h$	$C_v=0.5C_h$	$C_v=0.1C_h$
AIG	$V_x$ (m/sec)	6.10	6.10	6.10
	$\rho V_x$ ( $\text{kg}/\text{m}^2 \cdot \text{sec}$ )	2.68	2.68	2.68
	$D_m$ (%)	24.28	24.63	25.76
1 <sup>st</sup> Catalyst Layer	$V_x$ (m/sec)	3.20	3.20	3.20
	$\rho V_x$ ( $\text{kg}/\text{m}^2 \cdot \text{sec}$ )	2.09	2.09	2.09
	$D_m$ (%)	0.31	0.26	1.40
2 <sup>nd</sup> Catalyst Layer	$V_x$ (m/sec)	2.33	2.33	2.33
	$\rho V_x$ ( $\text{kg}/\text{m}^2 \cdot \text{sec}$ )	2.09	2.09	2.09
	$D_m$ (%)	0.32	0.37	0.59

fore, the behavior of  $\text{NH}_3$  gas with air is strongly dependent upon that of flue gas inevitably. If the same amount of  $\text{NH}_3$  with air for all AIG groups is injected, uneven  $\text{NH}_3$  concentration distribution

will be formed at the catalyst layer due to deviation of flue gas mass flux. This brings deterioration of performance and increase of  $\text{NH}_3$  slip. Therefore, if there is deviation of flue gas mass flux passing the AIG it is important to determine the  $\text{NH}_3$  feed rates for individual AIG groups considering flue gas mass flux in order to form a uniform  $\text{NH}_3$  concentration at the catalyst layer and to improve performance of SCR.

### 1-3. Determination of $\text{NH}_3$ Feed Rates for Individual AIG Groups

Determination of optimal  $\text{NH}_3$  feed rates for individual AIG branches can be done by considering flue gas mass flux passing through AIG. They are proportional to magnitudes of flue gas mass flux passing through the individual AIG branches. The flue gas mass flux was calculated by using CFD analysis at  $C_v=0.5C_h$  as an average behavior of flue gas. There is little difference between optimal  $\text{NH}_3$  feed rates for individual AIG branches based on flue gas mass flux and the values in real operations of commercial scale SCR because of minimum control limit of  $\text{NH}_3$  feed rate control valve. Four cases were prepared to apply for performance tests. CASE1 is to apply

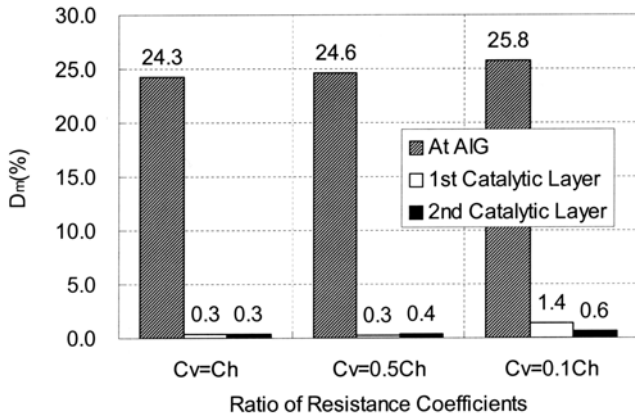


Fig. 11. Flue gas mass flux deviations for  $C_v=C_h$ ,  $C_v=0.5C_h$ , and  $C_v=0.1C_h$ : (▨) at AIG; (□) 1<sup>st</sup> catalytic layer; (■) 2<sup>nd</sup> catalytic layer.

the same feed rate of NH<sub>3</sub> for all AIG branches and it is prepared to compare with other three cases to apply different NH<sub>3</sub> feed rates considering the flue gas mass flux deviation. In CASE2, the 1<sup>st</sup>-5<sup>th</sup> AIG groups are operated without 6<sup>th</sup> AIG group, whereas all AIG groups are operated in CASE3 and CASE4. However, NH<sub>3</sub> feed rate through the 6<sup>th</sup> AIG group for CASE3 and CASE4 is different. In CASE3, it is maximum feed rate to be injected through the 6<sup>th</sup>

AIG group's pipe lines. In CASE4, NH<sub>3</sub> feed rate through the 6<sup>th</sup> AIG group is reduced to 33% of that in CASE3. NH<sub>3</sub> mass flow rates for each CASE are shown in Fig. 12.

**2. Performance Tests Using Individual AIG Groups**

Fig. 13 shows the CFD analysis results of NH<sub>3</sub> concentration distribution in case of individual AIG group operations. It shows that NH<sub>3</sub> concentration distribution and 1<sup>st</sup> catalyst area to be supplied with NH<sub>3</sub> are changed by NH<sub>3</sub> injection position. As shown in Table 3 and Fig. 14, there was much difference in NOx removal efficiencies and NH<sub>3</sub> slips although total NH<sub>3</sub> feed amounts for individual tests were almost the same. NOx removal efficiency has a tendency to be decreased as NH<sub>3</sub> slip becomes increased. It is a conflicting result in comparison with general catalyst properties. Fig. 15 shows the relationship between  $\rho V_x$  at individual AIG groups and  $D_c$  at the 1<sup>st</sup> catalyst layer. It is shown that  $D_c$  is inversely proportional to  $\rho V_x$  except for 1<sup>st</sup> AIG group, that is, when NH<sub>3</sub> was injected in heavy flue gas flowing region (4<sup>th</sup> and 5<sup>th</sup> AIG operations), NH<sub>3</sub> concentration distribution became relatively even at the catalyst layer and NOx removal efficiency was improved as shown in Fig. 16 and Fig. 17.

The main reason for these results can be explained by flue gas mass flux deviation at the AIG position and flue gas correction effect. If NH<sub>3</sub> is injected at the region, at which flue gas mass flux is high, some of the flue gas with NH<sub>3</sub> will be mixed with the flue gas without NH<sub>3</sub> by flue gas rising movement in front of the high pressure superheater. Thus, NH<sub>3</sub> can be supplied to more expanded

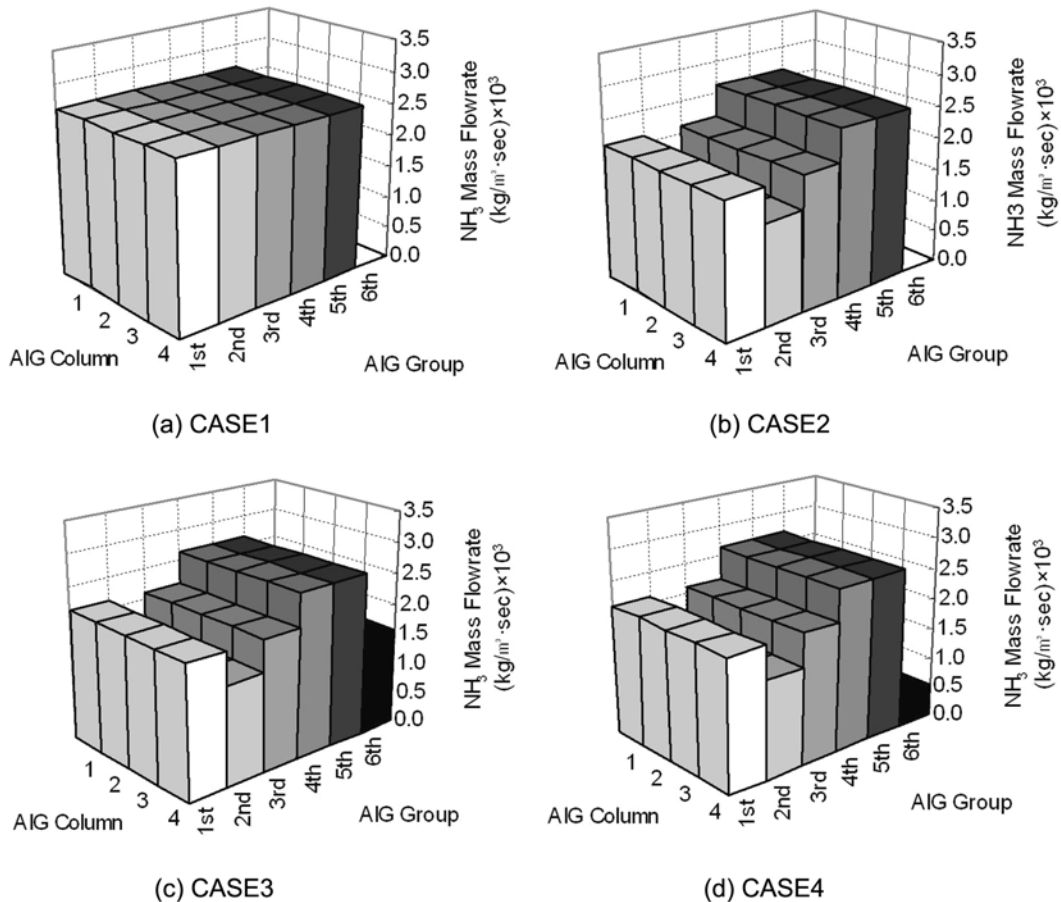


Fig. 12. NH<sub>3</sub> mass flowrates for individual AIG branches.

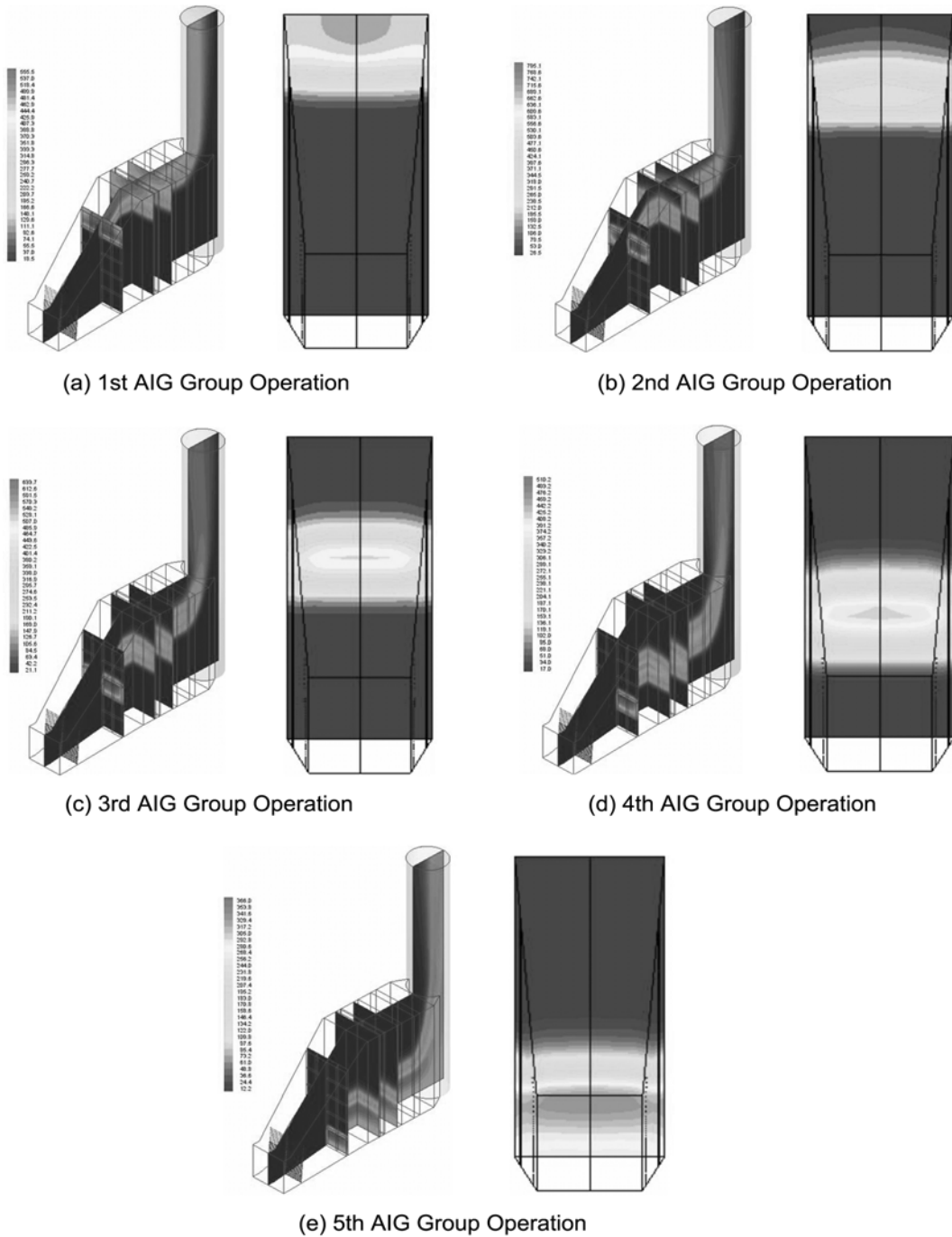


Fig. 13. CFD analysis results of  $\text{NH}_3$  concentration distribution for individual AIG group operation,  $C_v=0.5C_h$ : (left) total region; (right) 1<sup>st</sup> catalyst layer.

Table 3. Summary of experimental and CFD analytical results in case of individual AIG group operation

Operating AIG group	Experiment					CFD Analysis	
	Inlet NOx (ppm)	Outlet NOx (ppm)	NOx removal efficiency (%)	$\text{NH}_3$ slip (ppm)	$\text{NH}_3/\text{NOx}$	$\rho V_x$ at AIG ( $\text{kg}/\text{m}^2 \cdot \text{sec}$ )	$D_c$ at 1 <sup>st</sup> catalyst layer (%)
1 <sup>st</sup> Group	74.0	61.5	16.9	21.6	0.54	10.02	140.7
2 <sup>nd</sup> Group	79.8	65.4	18.1	11.3	0.48	7.07	128.8
3 <sup>rd</sup> Group	78.9	60.5	23.5	12.9	0.49	8.97	128.3
4 <sup>th</sup> Group	77.4	56.1	27.6	10.8	0.52	11.52	121.2
5 <sup>th</sup> Group	75.9	53.5	29.6	7.9	0.50	15.91	121.5

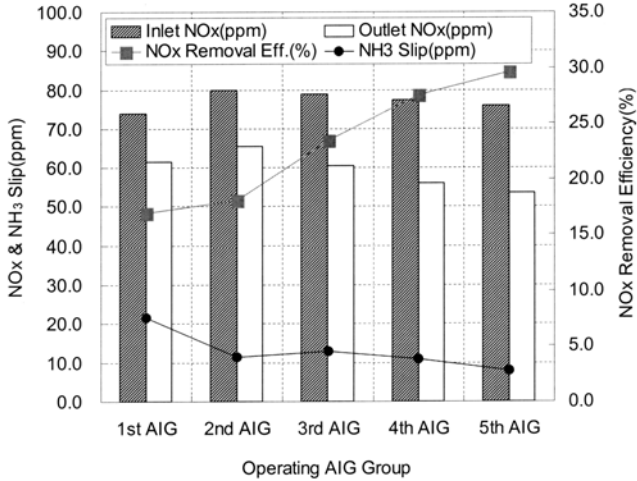


Fig. 14. Performance test result for individual AIG group operation: (▨) inlet NOx (ppm); (□) outlet NOx (ppm); (■) NOx removal efficiency (%); (○) NH<sub>3</sub> slip (ppm).

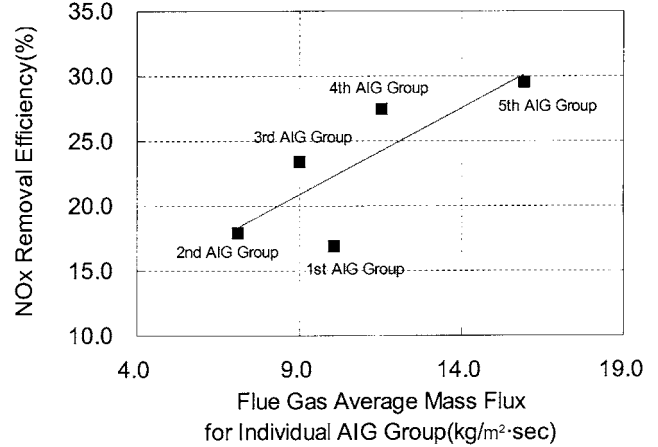


Fig. 16. Relationship between flue gas average mass flux,  $\rho V_x$  and NOx removal efficiency for individual AIG group operation.

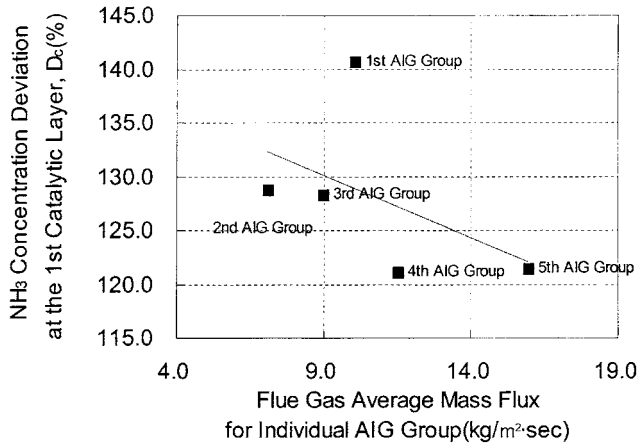


Fig. 15. Relationship between flue gas average mass flux,  $\rho V_x$  at individual AIG group and NH<sub>3</sub> concentration deviation, D<sub>c</sub> at the 1<sup>st</sup> catalyst layer for individual AIG group operation.

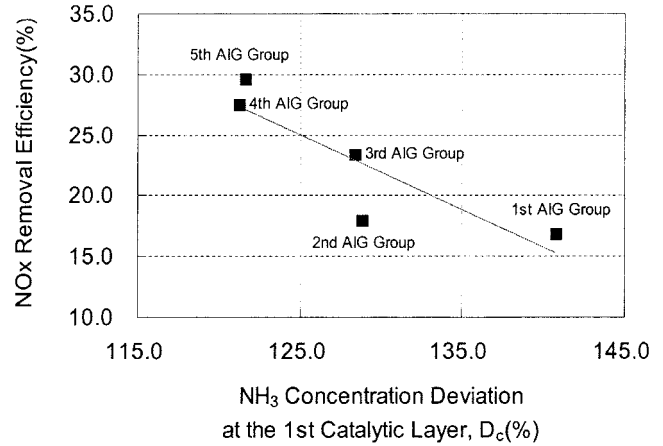


Fig. 17. Relationship between NH<sub>3</sub> concentration deviation, D<sub>c</sub> at the 1<sup>st</sup> catalyst layer and NOx removal efficiency for individual AIG group operation.

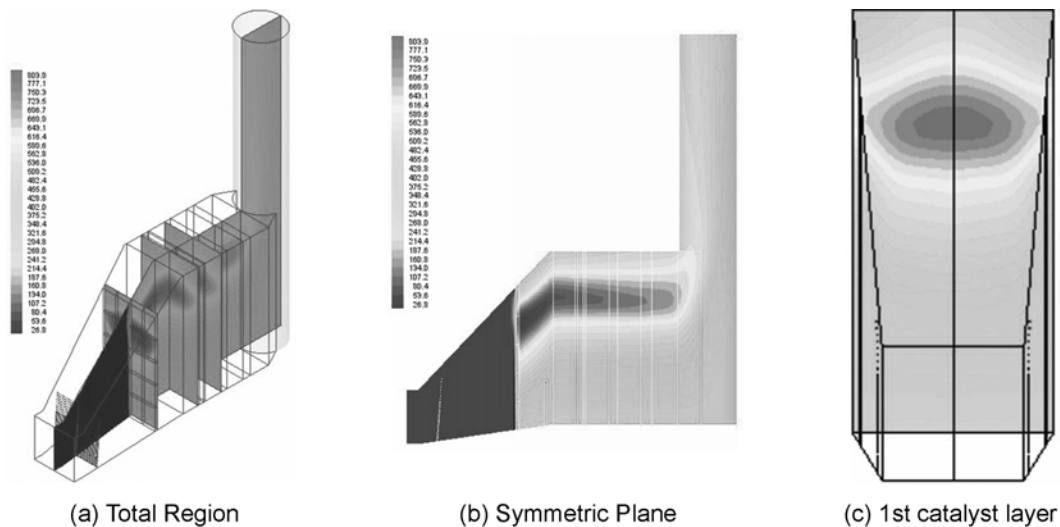


Fig. 18. CFD analysis result of NH<sub>3</sub> concentration distribution for performance test of CASE1, C<sub>v</sub>=0.5C<sub>h</sub>.

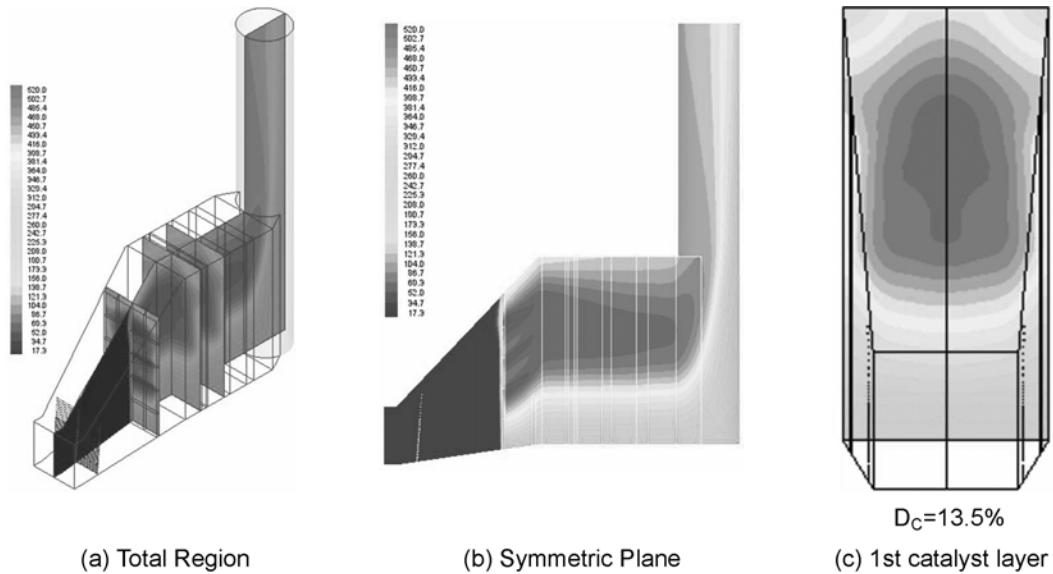


Fig. 19. CFD analysis result of  $\text{NH}_3$  concentration distribution for performance test of CASE2,  $C_i=0.5C_n$ .

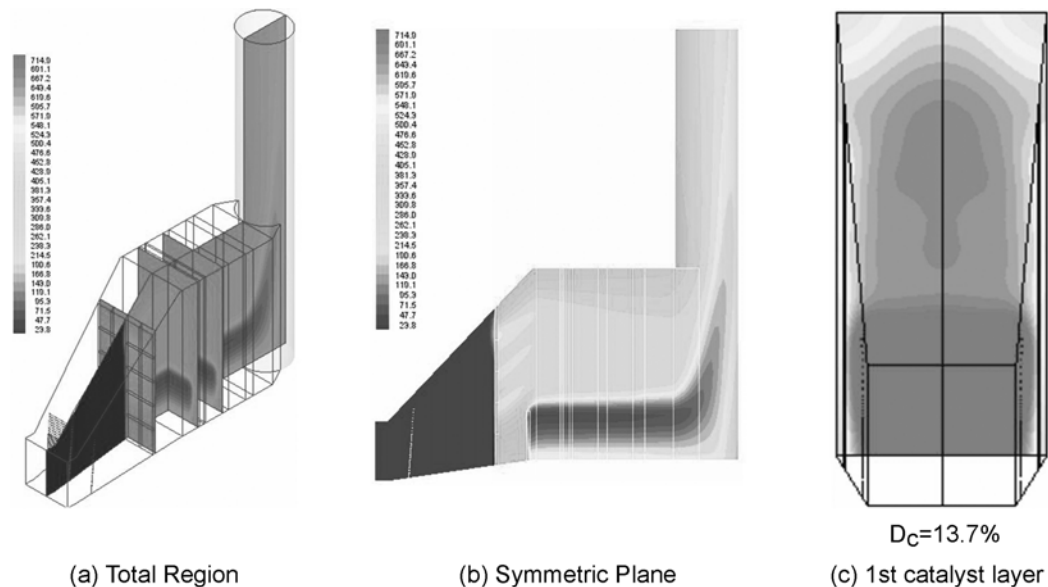


Fig. 20. CFD analysis result of  $\text{NH}_3$  concentration distribution for performance test of CASE3,  $C_i=0.5C_n$ .

catalyst area and most of the  $\text{NH}_3$  injected can react with  $\text{NO}_x$ . If  $\text{NH}_3$  is injected at the region, in which flue gas mass flux is low, the flue gas mixing amount between the flue gas with  $\text{NH}_3$  and the flue gas without  $\text{NH}_3$  will be reduced and it makes available catalyst area decreased and much of  $\text{NH}_3$  should flow out without  $\text{NO}_x$  reduction reaction. In addition, the extent of upward movement of flue gas in the upper part of HRSG is slight because of the ceiling. Thus, it is difficult to expect the flue gas mixing effect by rising movement of flue gas just as 4<sup>th</sup> and 5<sup>th</sup> AIG group operations in 1<sup>st</sup> AIG group operation.

The results of performance tests in individual AIG group operation and CFD analysis show that there is flue gas mass flux deviation in the inlet expansion duct of horizontal HRSG. Moreover,  $\text{NH}_3$  concentration deviation at the catalyst layer, available catalyst area and  $\text{NO}_x$  removal efficiency can be changed by flue gas mass flux

at the  $\text{NH}_3$  injection position. Therefore, it is concluded that  $\text{NH}_3$  feed rates for individual AIG groups should be determined in proportion to flue gas mass fluxes passing through individual AIG groups in order to maximize the performance of commercial scale SCR.

### 3. Performance Test Using All AIG Groups

CFD analysis results for  $\text{NH}_3$  concentration distribution inside HRSG are shown in Fig. 18, 19, 20 and 21. Table 4 and Fig. 22 are a summary of experimental results and  $\text{NH}_3$  concentration deviation,  $D_c$  at the 1<sup>st</sup> catalyst layer from CFD analysis for all cases. In CASE1,  $D_c$  at the 1<sup>st</sup> catalyst layer was 23.6%, which was the highest value out of all cases.  $\text{NO}_x$  removal efficiency in performance test was 54.4%. Average  $\text{NH}_3$  slip was 10.0 ppm during the experiment because SCR operation was done under constant  $\text{NH}_3$  slip, 10.0 ppm. Total  $\text{NH}_3$  average feed rate and  $\text{NH}_3/\text{NO}_x$  molar ratio is  $46.4 \text{ Nm}^3/\text{hr}$  and 0.565, which is the lowest value out of all cases. It is inter-

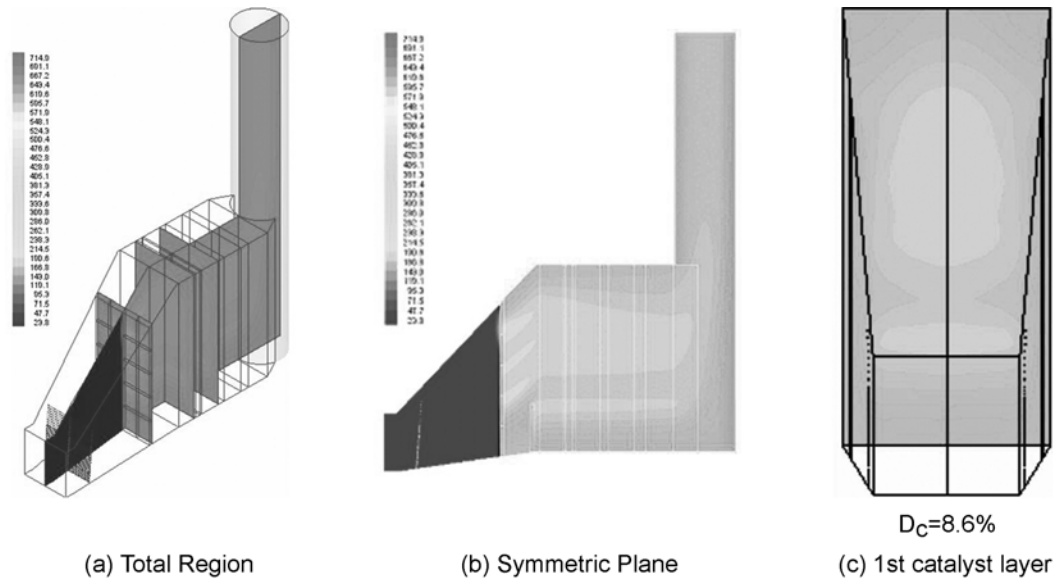


Fig. 21. CFD analysis result of  $\text{NH}_3$  concentration distribution for performance test of CASE4,  $C_r=0.5C_r$ .

Table 4. Summary of experimental and CFD analytical results in case of all AIG groups operation

CASE	Experiment						CFD analysis
	Inlet NOx (ppm)	Outlet NOx (ppm)	NOx removal efficiency (%)	$\text{NH}_3$ slip (ppm)	$\text{NH}_3$ feedrate ( $\text{Nm}^3/\text{hr}$ )	$\text{NH}_3/\text{NOx}$	$D_c$ at 1 <sup>st</sup> catalyst layer (%)
CASE1-1	114.8	53.5	53.4	10.0	48.6	0.54	23.6
CASE1-2	94.6	42.3	55.4	10.0	44.1	0.59	
CASE1 average	104.7	47.9	54.4	10.0	46.4	0.57	
CASE2-1	88.8	24.7	72.3	10.0	58.9	0.84	13.5
CASE2-2	98.4	30.1	69.2	10.2	60.8	0.80	
CASE2 average	93.6	27.4	70.8	10.1	59.8	0.82	
CASE3-1	79.4	31.8	60.0	10.1	48.9	0.78	13.7
CASE3-2	102.4	42.2	58.9	10.1	51.4	0.64	
CASE3 average	90.9	37.0	59.4	10.1	50.1	0.71	
CASE4-1	97.2	24.6	74.7	10.1	66.9	0.89	8.6
CASE4-2	99.6	24.9	75.0	10.1	64.1	0.81	
CASE4 average	98.4	24.8	74.8	10.1	65.5	0.85	

preted that there is excessive  $\text{NH}_3$  in upper catalyst layer and insufficient  $\text{NH}_3$  in the low catalyst layer because the same amount of  $\text{NH}_3$  for all AIG groups was injected without regard for flue gas mass flux deviation.  $D_c$  at the 1<sup>st</sup> catalyst layer in CASE2 was 13.5% and NOx removal efficiency was 70.8%.  $\text{NH}_3$  slip at the stack was 10.1 ppm. Total  $\text{NH}_3$  average feed rate was 59.8  $\text{Nm}^3/\text{hr}$  and  $\text{NH}_3/\text{NOx}$  molar ratio was 0.815. The operation results of CASE2 were more improved than those of CASE1. However, it seems that  $\text{NH}_3$  was deficient in the low part of HRSG as shown in Fig. 18. In CASE3, the 6<sup>th</sup> AIG group operation was introduced in order to solve the CASE2's problem.  $D_c$  at the catalyst layer is similar with CASE2 as 13.7% but NOx removal efficiency was 59.4% under  $\text{NH}_3$  slip of 10.1 ppm. Total  $\text{NH}_3$  average feed rate was 50.1  $\text{Nm}^3/\text{hr}$  and  $\text{NH}_3/\text{NOx}$  molar ratio was 0.708, which are less than those of CASE2. It seems that  $\text{NH}_3$  injected through the 6<sup>th</sup> AIG group brought about excessive  $\text{NH}_3$  in the lower part of catalyst layer and the excessive

$\text{NH}_3$  led to increase  $\text{NH}_3$  slip rapidly. Because it was necessary to find the optimal  $\text{NH}_3$  feed rate of the 6<sup>th</sup> AIG group in order to solve this problem,  $\text{NH}_3$  feed rate of the 6<sup>th</sup> AIG group in CASE4 was reduced to 33% of that in CASE3. In CASE4,  $D_c$  was 8.6% and NOx removal efficiency was 74.8%, which was the highest value among all cases.  $\text{NH}_3$  slip was 10.1 ppm. Total  $\text{NH}_3$  average feed rate was 65.5  $\text{Nm}^3/\text{hr}$  and  $\text{NH}_3/\text{NOx}$  molar ratio was 0.852. It means that  $\text{NH}_3$  deficiency or excess phenomena in the low part of catalyst layer in CASE2 and CASE3 were relieved.

From the results of performance test in all AIG groups operation and CFD analysis,  $D_c$  can be regulated by adjusting  $\text{NH}_3$  injection amounts for individual AIG groups, that is,  $\text{NH}_3$  concentration distribution can be homogeneous by means of injecting  $\text{NH}_3$  corresponding with flue gas mass flux. As shown in Fig. 23, NOx removal efficiency was increased as  $D_c$  at the catalyst layer became decreased. Therefore, it is concluded that  $\text{NH}_3$  injection amounts for individ-

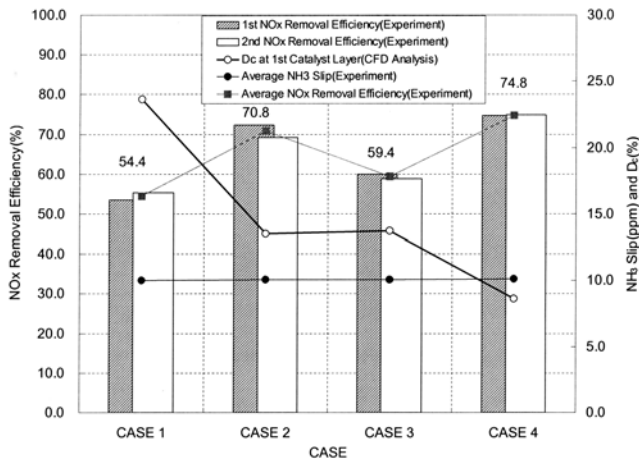


Fig. 22. Operating results for all AIG groups operation: (▨) NOx removal efficiency (1<sup>st</sup> experiment); (□) NOx removal efficiency (2<sup>nd</sup> experiment); (■) average NOx removal efficiency; (●)  $D_c$  at 1<sup>st</sup> catalyst layer (CFD analysis); (○) average NH<sub>3</sub> slip (experiment).

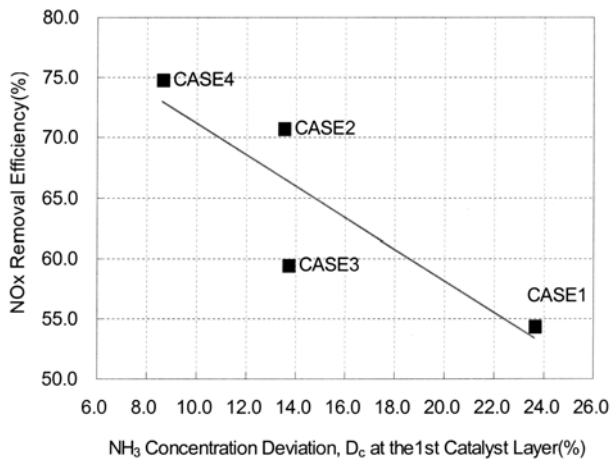


Fig. 23. Relationship between  $D_c$  at the 1<sup>st</sup> catalyst layer and NOx removal efficiency for all AIG groups operation.

ual AIG groups should be determined in accordance with flue gas mass flux passing through AIG in order to improve NOx removal efficiency. And CFD analysis method makes it possible to determine the optimal NH<sub>3</sub> feed rates for individual AIG groups easily.

## CONCLUSIONS

CFD analysis for commercial scale SCR installed in horizontal HRSG of combined cycle power plant was implemented. NH<sub>3</sub> injection method which could increase NOx removal efficiency was suggested and applied to real operations. The following conclusions were obtained from CFD analysis and experimental results.

Flue gas behavior inside HRSG was verified by using CFD analysis assuming that heat transfer pipe bundles are porous media. Primarily, flue gas behavior is corrected during passing through the existing flow correction device. However, flue gas distribution in the AIG region is still not even and most of flue gas flows through the low part of HRSG. In front of HPSH, strong upward movement of

flue gas occurs. Downstream of HPSH, flue gas behavior becomes very uniform.

As a result of applying different vertical resistance coefficients, it is proved that the porous media assumption is very effective in CFD analysis on HRSG and SCR. The flue gas and NH<sub>3</sub> concentration distribution at AIG and catalyst layer are quantified by using flue gas mass flux deviation,  $D_m$  and NH<sub>3</sub> concentration deviation,  $D_c$ .

From the experimental results, it was established that NH<sub>3</sub> injection corresponding with flue gas mass flux passing through AIG made it possible to form a homogeneous NH<sub>3</sub> concentration distribution at the catalyst layer and a uniform NH<sub>3</sub> concentration distribution at the catalyst layer contributed to improve the performance of commercial scale SCR. Computational fluid dynamics analysis method is very useful to determine the optimal NH<sub>3</sub> injection amounts for individual AIG groups which make NOx removal efficiency improved.

Finally, CFD analysis method can be applied to determine the optimal location of AIG and catalyst layer in case of the combined cycle power plant in which SCR catalyst and AIG should be installed inside the existing HRSG without additional SCR reactor. It is also expected that improved NOx removal efficiency can be obtained by applying different NH<sub>3</sub> feed rates for individual AIG groups based on flue gas mass flux (verified CFD analysis) if AIG should be installed where flue gas behavior is not uniform. Furthermore, it is expected that time and effort can be saved for system tuning and test operation.

## ACKNOWLEDGMENTS

The authors would like to thank the Korea Energy Management Corporation (KEMCO) for the financial support of this project (2001-C-CT06-P-01-0-000-2002).

## NOMENCLATURE

$t$	: time
$x_j$	: jth coordinate (if $j=1$ x, if $j=2$ y, if $j=3$ z)
$u_j$	: j direction velocity
$S_m$	: mass source term
$p$	: pressure
$g_j$	: acceleration of gravity
$F_j$	: momentum source term
$S_\phi$	: source of $\phi$
$\bar{w}$	: average velocity of main flow direction
$\bar{c}$	: average NH <sub>3</sub> concentration
$D$	: viscous resistance coefficient
$C$	: inertial resistance coefficient
$T$	: porous media thickness
$K_L'$	: real resistance coefficient of porous media
$A$	: cross section area by opening
$D_m$	: flue gas mass flux distribution deviation parameter
$D_c$	: NH <sub>3</sub> concentration distribution deviation parameter

## Greek Letters

$\rho$	: density
$\mu$	: kinematic viscosity of fluid

$\phi$  : scholar variable  
 $\Gamma$  : diffusion coefficient  
 $\alpha$  : permeability [ $\text{m}^2$ ]

## REFERENCES

- Adams, B., Cremer, M., Valentine, J., Bhamidipati, V., Letcavits, J., O'Connor, D. and Vierstra, S., *Use of CFD modeling for design of NOx reduction systems in utility boilers*, Proceeding of the 2002 International Joint Power Generation Conference, ASME, Phoenix, AZ (2002).
- Arbind, P., "Air pollution control technologies for nitrogen oxides," *The National Environmental Journal*, **46**, May (1995).
- Bruce, I., "NOx reduction techniques," *The American Ceramic Society Bulletin*, **81**, Oct. (1995).
- Fluent User's Guide, Version 6.1; Fluent: Lebanon, NH (1998).
- Freek, K., Lydia, S., Nico, J. J. D. and Jacob, A. M., "Kinetics of the selective catalyst reduction of NO with NH<sub>3</sub> over Mn<sub>2</sub>O<sub>3</sub>-WO<sub>3</sub>-Al<sub>2</sub>O<sub>3</sub>," *Ind. Eng. Chem. Res.*, **44**, 32 (1993).
- Heck, R. M., Chen, J. M. and Speronello, B. K., "Operating characteristics and commercial operating experience with high temperature SCR NOx catalyst," *Environmental Progress*, **22**, 13 (1994).
- Jaime, B., *Progress engineering and design for air pollution control*, Prentice Hall, New Jersey (1993).
- Jiri, S., Natale, F., Pio, F., Enrico, T. and Fiorenzo, B., "Selective reduction of NOx by NH<sub>3</sub> over honeycomb DeNOxing catalysts," *Ind. Eng. Chem. Res.*, **10**, 32 (1993).
- Kenneth, J. F. and John, H. C., "Design guidelines for NH<sub>3</sub> injection grids; optimize SCR NOx removal," *Oil & Gas Journal*, **56**, Nov. (1993).
- Kevin, R., Mel, A. and Michael, V., *Numerical modeling for design optimization of SCR applications*, ICAC NOx Forum Washington D.C. (2000).
- Kevin, R., Milobowski, M. and Wooldridge, B., *Perspectives on ammonia injection and gaseous static mixing in SCR retrofit applications*, EPRI-DOE-EPA Combined Utility Air Pollutant Control Symposium, Washington D.C. (1999).
- Kokkinos, A., Nelson, N. and Stürgwolt, W., *Structural considerations for SCR retrofits*, EPRI-DOE-EPA Combined Utility Air Pollutant Control Symposium, Washington D.C. (1999).
- Kotter, M. and Lintz, H. G., "Selective catalyst reduction of nitrogen oxides - an original concept," *International Chemical Engineering*, **68**, 31 (1991).
- Lauder, B. E. and Spalding, D. B., *Mathematical models of turbulence*, Academic Press, London, England (1972).
- Pantankar, S. V., *Numerical heat transfer and fluid flow*, Hemisphere Publishing Corporation, Washington D.C. (1980).
- Ralf, S., Cindy, K. and Edward, H., "Enhance ammonia distribution for maximum SCR performance," *Institute of Clean Air Companies Forum 2003*, **4**, Oct. (2003).
- Sayre, A. and Milobowski, M., *Validation of numerical models of flow through SCR units*, EPRI-DOE-EPA Combined Utility Air Pollutant Control Symposium, Washington D.C. (1999).